Inorganic Chemistry
Article
Cite This: Inorg. Chem. XXXX, XXX, XXX−XXX
pubs.acs.org/IC

Unexpected Magnetic Ordering on the Cr Substructure in UCr_2Si_2C and Structural Relationships in Quaternary U-Cr-Si-C Compounds

Pierric Lemoine,*[,§] Anne Vernière,[‡] Mathieu Pasturel,[§] Gérard Venturini,[‡] and Bernard Malaman[‡]

[§]Univ. Rennes, CNRS, ISCR-UMR 6226, F-35000 Rennes, France

[‡]Institut Jean Lamour, UMR-CNRS 7198, Université de Lorraine, Faculté des Sciences et Technologies, B.P. 70239, 54506 Vandœuvre-lès-Nancy Cedex, France

Supporting Information

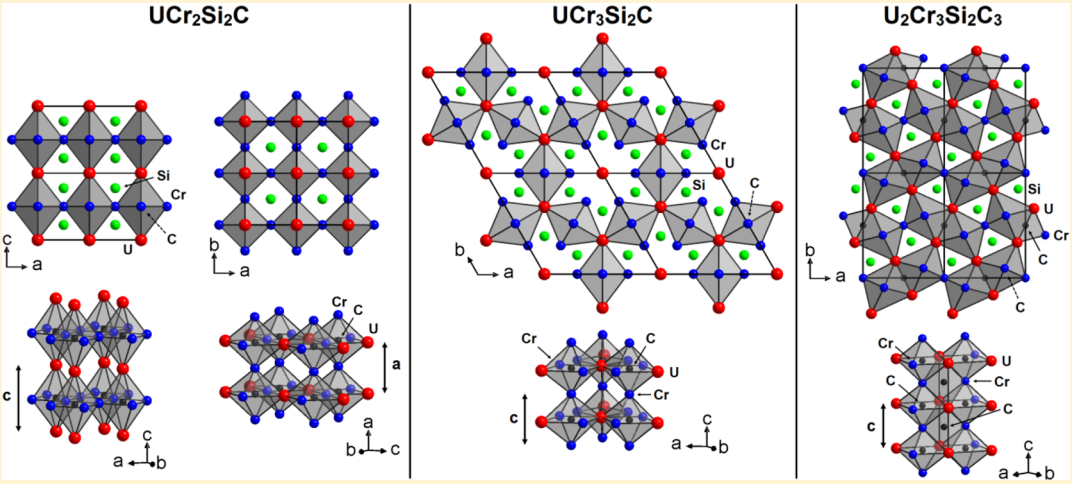

ABSTRACT: Previous experimental and theoretical studies revealed that carbon insertion into the RCr_2Si_2 compounds drastically affects the magnetic behavior, since chromium does not carry any magnetic moment in RCr_2Si_2C (R = Y, La−Sm, Gd−Er) compounds in contrast to RCr_2Si_2 (R = Y, Sm, Gd−Lu, Th) compounds. In this study, we report on the unexpected magnetic ordering of chromium atoms in the isotype quaternary UCr_2Si_2C compound. While specific heat and magnetic measurements suggest a Pauli paramagnetic behavior, neutron powder diffraction reveals an antiferromagnetic ordering of the chromium substructure at high temperature (T_N > 300 K), while that of uranium remains nonmagnetically ordered down to 2 K. Its magnetic behavior, inverse in comparison to the RCr_2Si_2C carbides involving a magnetic lanthanide, is discussed in relation with the singularity of its crystal structure among the series. Moreover, the crystallographic structures and the structural stability of UCr_2Si_2C and of two other quaternary U-Cr-Si-C compounds (i.e., UCr_3Si_2C and $U_2Cr_3Si_2C_3$), based on the full occupancy of interstitial sites by carbon atoms, are discussed and compared to those of the related ternary intermetallics. Finally, the low-temperature form of UCr_2Si_2, corresponding to a displacive transformation around 210 K of the $ThCr_2Si_2$-type structure, is reinvestigated by considering a higher symmetry monoclinic unit cell ($C2/m$) instead of the previously reported triclinic cell ($P\bar{1}$). The antiferromagnetic ordering at low temperature (T_N = 30(2) K) of the uranium substructure is confirmed, and its magnetic structure is reanalyzed and discussed considering the monoclinic crystal structure.

INTRODUCTION

The ternary RT_2X_2 compounds (R = lanthanide; T = 3d, 4d, or 5d transition metal; X = Si, Ge), with the $ThCr_2Si_2$ structure type ($I4/mmm$),[1] have been intensely studied for their wide range of electronic properties such as intermediate valence, heavy-Fermion behavior, and superconductivity.[2] It has been considered for a long time that among these compounds only those with T = Mn exhibit a magnetic ordering of the transition-metal substructure.[2−4] Indeed, for T = Fe, Co, Ni, the compounds involving a diamagnetic R element (i.e., Y, La, Lu) are weak Pauli paramagnets, indicating that the T atoms do not carry any magnetic moment.[5−9] In contrast, the RMn_2X_2 compounds (R = Y, La, Lu; X = Si, Ge) order magnetically at high temperature,[10−14] indicating a magnetic ordering of the Mn substructure: an antiferromagnetic order is observed from T_N down to the lowest reached temperature for the compounds with R = Y, Lu,[15−18] while $LaMn_2X_2$ undergoes an antiferro- to ferromagnetic transition below T_N.[12,18,19]

The magnetic behavior of the RCr_2Si_2 (R = Y, Sm, Gd−Lu, Th) series is more ambiguous. YCr_2Si_2, $LuCr_2Si_2$, and $ThCr_2Si_2$ have first been reported to be Pauli paramagnets, suggesting

Received: November 15, 2017

DOI: 10.1021/acs.inorgchem.7b02901
Inorg. Chem. XXXX, XXX, XXX−XXX

Table 1. Refined Atomic Coordinates, Site Occupancies, and Isotropic and Anisotropic Displacement Parameters of UCr_2Si_2-RT and UCr_2Si_2C[a]

atom	site	x	y	z	occ	U_{11}	U_{22}	U_{33}	U(eq)
					UCr_2Si_2 (R1 = 0.63%)				
U	2a	0	0	0	1.00	0.0061(1)	U_{11}	0.0090(2)	0.0071(1)
Cr	4d	0	1/2	1/4	1.00	0.0125(2)	U_{11}	0.0073(2)	0.0107(2)
Si	4e	0	0	0.3862(2)	1.00	0.0085(3)	U_{11}	0.0121(4)	0.0097(2)
					UCr_2Si_2C (R1 = 1.54%)				
U	1a	0	0	0	1.00	0.0024(2)	U_{11}	0.0052(2)	0.0033(2)
Cr	2e	0	1/2	1/2	1.00	0.0017(5)	0.0035(5)	0.0054(4)	0.0035(2)
Si	2h	1/2	1/2	0.2247(4)	1.00	0.0038(5)	U_{11}	0.0050(7)	0.0042(3)
C	1b	0	0	1/2	1.00	0.006(2)	U_{11}	0.013(4)	0.008(2)

[a] $U_{12} = U_{13} = U_{23} = 0$.

that the chromium atoms carry no magnetic moment.[20−22] However, magnetic measurements on the solid solutions $RFe_{2-x}Cr_xSi_2$ (R = Y, La, Nd, Tb)[23] have shown that the Cr substructure orders antiferromagnetically at very high temperature (T_N > 600 K). This behavior was finally confirmed by neutron diffraction studies,[24−26] which evidence an antiferromagnetic layer (AFl) arrangement and a large magnetic moment on the Cr atoms (∼1.6 μ_B). In this series, the lanthanide substructure of compounds involving a paramagnetic lanthanide appears to be magnetically ordered at very low temperature (<2.5 K).[21,24,25,27−29]

Among the RCr_2Si_2 series, UCr_2Si_2 appears to be unique. It crystallizes in the $ThCr_2Si_2$ structure type at room temperature and presents a structural transition (T_t = 210 K) from the high-symmetry tetragonal $I4/mmm$ space group to the low-symmetry triclinic $P\bar{1}$ space group.[30] The low-temperature form of UCr_2Si_2 was already reported by Matsuda et al. to be a very weak deformation of the tetragonal unit cell described by a very small tilt of the c axis toward the [1,−1,0] direction (0.7°).[30] However, the crystal structure results presented by these authors appear ambiguous: the Cr and Si atomic coordinates reported in the triclinic structure do not correspond to a weak deformation of the $ThCr_2Si_2$ type, while the uranium atoms (1a (0,0,0) and 1h (1/2,1/2,1/2) sites) are connected by a body-centered Bravais lattice. Finally, in this compound, the chromium substructure is nonmagnetic, while that of uranium orders antiferromagnetically below T_N = 30 K.[22,30]

Addition of carbon to the previous series induces (i) the formation of the quaternaries RCr_2Si_2C (R = Y, La−Sm, Gd−Er), which crystallize in the $CeCr_2Si_2C$-type of structure ($P4/mmm$), a variant of the $CeMg_2Si_2$-type by the full occupation of the 1b site by carbon atoms[31,32] and (ii) a change of the type of magnetic behavior with (a) a subsequent ferromagnetic ordering of the lanthanide substructure at low temperature ($T_C \leq$ 30 K) for R = Pr, Nd, Gd−Dy[33−37] and (b) no magnetic moment detected on the chromium substructure.[33,37] It is worth noting that no quaternary UCr_2Si_2C carbide has ever been reported.

Considering (i) the ambiguous results reported for the low-temperature crystal structure of UCr_2Si_2, (ii) the singular magnetic behavior of UCr_2Si_2 in comparison to the other members of the series, and (iii) the absence of structural and magnetic data on UCr_2Si_2C, we have decided to (re)analyze the crystal and magnetic structures of UCr_2Si_2 and of the new UCr_2Si_2C quaternary compound by using powder and single-crystal X-ray diffraction, magnetic and heat capacity measurements, and powder neutron diffraction. Moreover, during this study, we have determined by single-crystal X-ray diffraction the crystallographic structures of two other intermetallics discovered in the U-Cr-Si-C quaternary system: UCr_3Si_2C[38] and $U_2Cr_3Si_2C_3$. All of the results are reported and discussed in this paper.

EXPERIMENTAL METHODS

Synthesis. Polycrystalline samples of UCr_2Si_2, UCr_2Si_2C, and UCr_3Si_2C were prepared by starting from high-purity elements (≥99.9 wt %). Pure elements were melted in a water-cooled copper crucible using a high-frequency induction furnace under an argon atmosphere. The UCr_2Si_2C sample was finely ground, compacted into a pellet, sealed in a silica tube under an argon atmosphere, and annealed at 1373 K for 1 month in a tubular furnace. The purity and chemical composition of each sample were checked by microprobe analysis (Cameca SX 100) at the Service Commun de Microscopies Électroniques et de Microanalyses de l'Université de Lorraine.

Powder X-ray and Neutron Diffractions. The crystal structure and the presence of impurities in the samples were checked at room temperature by powder X-ray diffraction (PXRD) using filtered Cu Kα radiation and a reflection Bragg−Brentano θ−θ geometry (Philips X-Pert Pro) diffractometer. Low-temperature (T = 150 K) patterns were recorded with the aid of a liquid nitrogen cryostat. Microprobe and PXRD analyses indicated that the UCr_2Si_2 sample is single-phase while the UCr_2Si_2C sample contains small quantities of the UCr_3Si_2C compound. The UCr_2Si_2C and UCr_3Si_2C samples contained small quantities of a new quaternary $U_2Cr_3Si_2C_3$ compound (see below).

Powder neutron diffraction (PND) experiments were carried out at the Institut Laue Langevin (ILL), Grenoble, France. The data were collected from 300 K down to ∼2 K using the high-flux neutron two-axis powder diffractometer D1B (λ = 2.52 Å) equipped with a one-dimensional curved multidetector.

The analysis of the PXRD and PND patterns was performed by Rietveld refinement using the FullProf and WinPlotr software packages.[39,40]

Single-Crystal X-ray Diffraction. Small single crystals ($\phi \approx$ 30 μm) of UCr_2Si_2, UCr_2Si_2C, and UCr_3Si_2C were extracted from the as-cast ingots. From the UCr_3Si_2C ingot, it has also been possible to extract very small single crystalline shards ($\phi \approx$ 10 μm) whose $U_2Cr_3Si_2C_3$ chemical composition was deduced from the XRD data (see below). Diffraction data were collected at room temperature on a Bruker APEX II-CCD area detector X-ray diffractometer equipped with a fine-focus source (Mo Kα, λ = 0.71073 Å) at the Centre de Compétence X-Gamma of the Institut Jean Lamour in Nancy, France. An extra measurement at low temperature (T = 100 K) was performed on the UCr_2Si_2 single crystal in order to reanalyze its low-temperature crystal structure. The structures were solved by direct methods using the SIR97 program[41] and then refined with full-matrix least-squares methods based on F^2 (SHELXL-2014)[42] using the WinGX software package.[43] All atoms were refined with anisotropic atomic displacement parameters. The reported data were computed using the CRYSCALC program.[44] The conditions of data collection and

DOI: 10.1021/acs.inorgchem.7b02901
Inorg. Chem. XXXX, XXX, XXX−XXX

structure refinements are gathered in Table S1 in the Supporting Information.

Further details of the crystal structure investigations may be obtained from FIZ Karlsruhe, 76344 Eggenstein-Leopoldshafen, Germany (fax: (+49)7247−808−666; e-mail: crysdata@fiz-karlsruhe.de, on quoting the deposition numbers CSD-432802, CSD-432803, CSD-432804, CSD-432805, and CSD-432806.

Magnetic Measurements. Zero-field-cooled (ZFC) magnetic measurements were carried out on powder samples from 5 to 300 K using a PPMS-9 system (Quantum Design) in an applied magnetic field of 0.25 T. This device was also used to perform magnetization measurements in fields up to 9 T.

Heat Capacity Measurements. Extra bulky samples of UCr_2Si_2C, UCr_3Si_2C, and $U_2Cr_3Si_2C_3$ were prepared by arc melting and annealed for 3 weeks at 1273 K. These samples were then cut into rectangular ingots for heat capacity measurements on a PPMS (Quantum Design) platform using a thermal relaxation method from room temperature down to 2 K.

RESULTS AND DISCUSSION

Room-Temperature Single-Crystal X-ray Diffraction. *UCr_2Si_2-RT.* Single-crystal X-ray diffraction refinement at room temperature confirms that the ternary UCr_2Si_2-RT compound crystallizes in the $ThCr_2Si_2$ type of structure ($I4/mmm$)[45] with the refined lattice parameters a = 3.910(1) Å and c = 10.501(1) Å (Table S1 in the Supporting Information). In this crystal structure, U, Cr, and Si atoms are located on the 2a (0,0,0), 4d (0,1/2,1/4), and 4e (0,0,z_{Si}) sites, respectively (Table 1). All sites are fully occupied by the respective atoms. A representation of the crystal structure is shown in Figure 1.

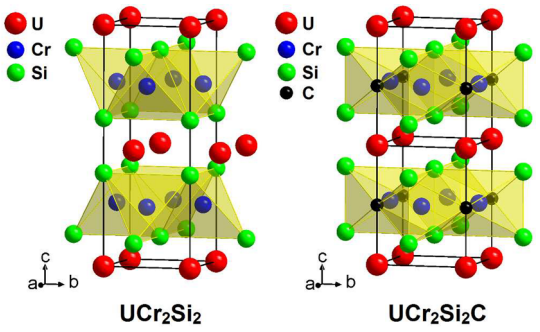

Figure 1. Crystal structure representations of UCr_2Si_2-RT and UCr_2Si_2C (doubled unit cell along the c axis for the latter).

UCr_2Si_2C. The structural refinement performed on the single-crystal X-ray diffraction data of UCr_2Si_2C indicates that this new quaternary compound crystallizes in the $CeCr_2Si_2C$ structure type ($P4/mmm$),[31] with the refined lattice parameters a = 3.983(1) Å and c = 5.160(1) Å (Table S1 in the Supporting Information). In this crystal structure, U, Cr, Si, and C atoms are located on the 1a (0,0,0), 2e (0,1/2,1/2), 2h (1/2,1/2,z_{Si}), and 1b (0,0,1/2) sites, respectively (Table 1). The refinement indicates a full occupancy of the U, Cr, and Si sites. Due to the presence of heavy atoms (U, Cr, Si), the localization of the carbon atoms and the rate occupancy of their site cannot be determined unambiguously by X-ray diffraction. However, the coherent neutron scattering length of carbon (+6.648 fm) allows us to distinguish this element among uranium (+8.61 fm), chromium (+3.635 fm), and silicon (+4.159 fm) atoms. Thus, from Rietveld refinement of the UCr_2Si_2C PND pattern (see below), we confirm unambiguously that, in this compound, carbon atoms fully occupy the 1b (0,0,1/2) site (Table 1). A representation of the crystal structure is shown in Figure 1.

UCr_3Si_2C. The structural refinement performed on the single-crystal XRD data of UCr_3Si_2C confirms that this quaternary compound crystallizes in the YCr_3Si_2C structure type ($P6/mmm$),[38] with the refined lattice parameters a = 8.968(1) Å and c = 4.003(1) Å (Table S1 in the Supporting Information). In this crystal structure, U atoms fully occupy the 2d (1/3,2/3,1/2) site and partially occupy the 1a (0,0,0) and 2e (0,0,z_U) sites, Cr atoms fully occupy the 6k (x_{Cr},0,1/2) and 3f (1/2,0,0) sites, silicon atoms fully occupy a 6l (x_{Si},2x_{Si},0) site, and carbon atoms fully occupy the 3g (1/2,0,1/2) site (Table 2). As in the case of UCr_2Si_2C, the localization and rate occupancy of carbon atoms on the 3g site have been confirmed by powder neutron diffraction (see below). A projection of the crystal structure of UCr_3Si_2C is shown in Figure 2.

$U_2Cr_3Si_2C_3$. Single-crystal shards of $U_2Cr_3Si_2C_3$ were extracted from the UCr_3Si_2C as-cast ingot and characterized by single-crystal X-ray diffraction. This new quaternary compound crystallizes in the orthorhombic $Pbam$ space group with the refined lattice parameters a = 7.052(3) Å, b = 9.106(3) Å, and c = 3.957(2) Å (Table S1 in the Supporting Information). The structural model deduced from SIR97[41] indicates that U atoms are located on a 4g (x_U,y_U,0) site, Cr atoms on a 4h (x_{Cr},y_{Cr},1/2) and 2a (0,0,0) sites, and Si atoms on a 4h (x_{Si},y_{Si},1/2) site (Table 2), yielding the chemical formula $U_2Cr_3Si_2$.

However, at this point, weak positive residual electron differences were detected on second 4g (x,y,0) and 2d (0,1/2,1/2) sites, suggesting the presence of light atoms on these positions. Considering the fact that the single crystal was extracted from the UCr_3Si_2C ingot, the occurrence of carbon atoms on these positions was assumed (Table 2). The final refinement indicates a full occupancy of these two crystallographic sites, leading to the structural formula $U_2Cr_3Si_2C_3$, with a final R1 value of 0.0156 and largest residual peak and hole of +1.74 and −1.36 e Å^{-3} (Table S1 in the Supporting Information). This structural model was introduced in the refinement of the PND data measured on the UCr_3Si_2C sample and allow a fit of the extra diffraction peaks observed on the pattern. A projection of the crystal structure of $U_2Cr_3Si_2C_3$ is shown in Figure 3.

Discussion of the Crystal Structure Stability. *UCr_2Si_2-RT and UCr_2Si_2C.* The results of the structure refinements indicate that the insertion of carbon atoms within the chromium square planes induces an increase in the a lattice parameter (+1.9%) and, in contrast, a decrease in the c lattice parameter (−1.7%) of UCr_2Si_2C in comparison to half those of UCr_2Si_2-RT. These results are in agreement with those previously reported by Klosek et al. on the RCr_2Si_2 and RCr_2Si_2C (R = Sm, Gd−Er) series.[33] Room-temperature interatomic distances in UCr_2Si_2-RT and UCr_2Si_2C, calculated from the single-crystal refinements, are gathered in Table S2 in the Supporting Information. Their relative evolutions have been calculated from the relation $\Delta_{ij} = 100[d_{ij} - (r_i + r_j)]/(r_i + r_j)$, where d_{ij} is the interatomic distance between i and j atoms with r_i and r_j the respective metallic radii evaluated by Teatum et al. (i.e., r_U = 1.56 Å, r_{Cr} = 1.36 Å, r_{Si} = 1.319 Å, and r_C = 0.916 Å).[46] These calculations evidence that the crystal structure stabilities of both UCr_2Si_2-RT and UCr_2Si_2C are mainly linked to the existence of strong Cr−Si and Si−Si chemical bonding. For the latter, the stability is also related to the presence of carbon atoms within the chromium square

DOI: 10.1021/acs.inorgchem.7b02901
Inorg. Chem. XXXX, XXX, XXX−XXX

Table 2. Refined Atomic Coordinates, Site Occupancies, and Isotropic and Anisotropic Displacement Parameters of UCr_3Si_2C and $U_2Cr_3Si_2C_3$ at Room Temperature[a]

atom	site	x	y	z	occ	U_{11}	U_{22}	U_{33}	U_{12}	U(eq)
					$U_{0.89}Cr_3Si_2C$ (R1 = 2.25%)					
U	2d	1/3	2/3	1/2	1.00	$2U_{12}$	$2U_{12}$	0.0027(2)	0.0023(1)	0.0040(1)
U	1a	0	0	0	0.54(1)	$2U_{12}$	$2U_{12}$	0.0110(4)	0.0025(2)	0.0070(2)
U	2e	0	0	0.290(2)	0.07(1)	$2U_{12}$	$2U_{12}$	0.011(3)	0.0067(9)	0.013(2)
Cr	6k	0.2825(1)	0	1/2	1.00	0.0051(2)	$2U_{12}$	0.0020(3)	0.0023(2)	0.0040(2)
Cr	3f	1/2	0	0	1.00	0.0051(3)	$2U_{12}$	0.0023(5)	0.0027(2)	0.0042(2)
Si	6l	0.1881(2)	2x	0	1.00	0.0058(4)	$2U_{12}$	0.0028(6)	0.0036(3)	0.0051(2)
C	3g	1/2	0	1/2	1.00	0.005(2)	$2U_{12}$	0.003(3)	0.002(2)	0.0044(12)
					$U_2Cr_3Si_2C_3$ (R1 = 1.56%)					
U	4g	0.3974(1)	0.1613(1)	0	1.00	0.0030(2)	0.0045(2)	0.0038(1)	−0.0008(1)	0.0038(1)
Cr	4h	0.2429(2)	0.4076(1)	1/2	1.00	0.0031(4)	0.0044(3)	0.0032(3)	−0.0002(3)	0.0036(2)
Cr	2a	0	0	0	1.00	0.0038(5)	0.0033(4)	0.0035(4)	0.0004(4)	0.0035(2)
Si	4h	0.0906(2)	0.1527(2)	1/2	1.00	0.0037(7)	0.0043(6)	0.0045(6)	−0.0002(5)	0.0041(3)
C	4g	0.2391(8)	0.4022(6)	0	1.00	0.009(3)	0.013(2)	0.007(2)	−0.004(2)	0.0095(10)
C	2d	0	1/2	1/2	1.00	0.026(6)	0.034(5)	0.025(5)	0.006(5)	0.028(2)

[a] $U_{13} = U_{23} = 0$.

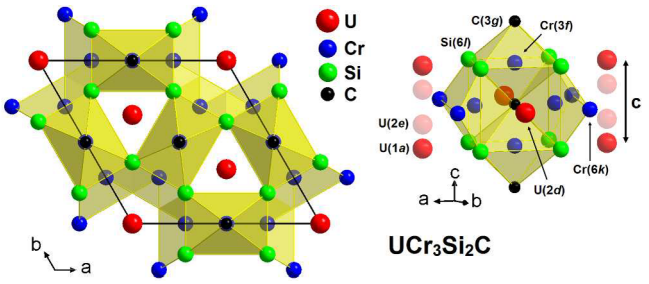

Figure 2. (left) Projection of the crystal structure of UCr_3Si_2C along the c axis and (right) detail of this structure around the carbon atom.

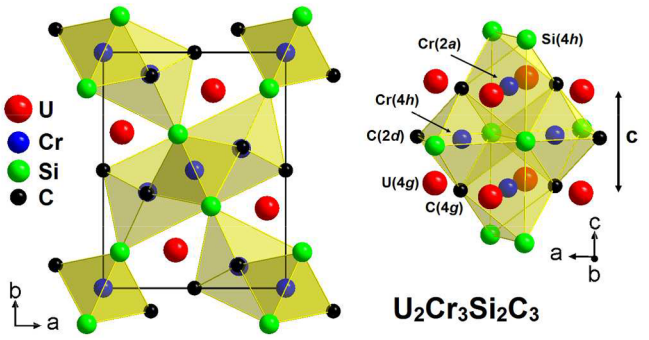

Figure 3. (left) Projection of the crystal structure of $U_2Cr_3Si_2C_3$ along the c axis and (right) detail of the structure highlighting the chromium atom environments.

planes, leading to strong Cr−C chemical bonding. Similar results were reported on the RCr_2Si_2C (R = Y, La, Sm) carbides.[33] The authors also reported the existence of covalent R−C bonds (and to a lesser extent R−Si bonds) in RCr_2Si_2C (R = Y, La, Sm), explaining the contraction of the c lattice parameter of these compounds in comparison to half that of RCr_2Si_2.[33] In contrast, UCr_2Si_2C is characterized by non-negligible positive relative evolutions of the interatomic distances between uranium and carbon atoms on the one hand and between uranium and silicon atoms on the other hand (Table S2 in the Supporting Information), despite the fact that UCr_2Si_2C evidences the smallest c lattice parameter and c/a ratio (1.296) of the RCr_2Si_2C series. Thus, the positive values of ΔU−C and ΔU−Si suggest that the contraction of the c lattice parameter of UCr_2Si_2C in comparison to half that of UCr_2Si_2-RT is related to strong chemical bonds in the Si-(Cr,C)-Si block. Such discrepancies between rare-earth- and uranium-based isostructural intermetallics are mostly due to the much smaller metallic radius of uranium in comparison to lanthanides.

UCr_3Si_2C. The main interatomic distances and their relative evolutions, calculated from single-crystal refinement (Table S3 in the Supporting Information) suggest that the crystal stability of this compound results from strong Cr−Cr, Cr−Si, and Cr−C chemical bonds. In contrast, they clearly indicate the absence of chemical bonding between Si atoms on the one hand and between Si and C atoms on the other hand. Similar results were reported on YCr_3Si_2C.[38] However, in this latter compound, relatively short interatomic distances between Y atoms and both Si and C atoms (Δ < 0) suggest weak Y−Si and Y−C chemical bonds, which is not the case in UCr_3Si_2C. This scenario where all uranium to ligand distances are exceeding the sum of the metallic radii is frequently observed not only in the (i) "cage"-like aluminides such as UT_2Al_{10},[47] UT_2Al_{20}[48] and borides such as UB_{12}[49] but also in the (ii) silicides such as USi_2,[50] UCr_2Si_2,[45] and $U_{20}Si_{16}C_3$ (around the U atoms in 1a and 1b positions) and $U_3Si_2C_2$ (around the U atom in the 2a site).[51]

$U_2Cr_3Si_2C_3$. The main interatomic distances and their relative evolutions, calculated from single-crystal refinement (Table S4 in the Supporting Information), indicate that the crystal stability of $U_2Cr_3Si_2C_3$ results from strong Cr−Si and Cr−C chemical bonds. Moreover, these calculations suggest weak U−C and U−Si chemical bonds. Finally, they clearly indicate the absence of chemical bonding between Si atoms on the one hand and between Si and C atoms on the other hand. Thus, this compound evidences strong chemical bonds both in the (00*l*) atomic planes (z = 0 and z = 1/2) and between them (Figure S1 in the Supporting Information) allowing us to conclude a three-dimensional stability of the crystallographic structure.

Considering the shortest interatomic distances calculated from single-crystal X-ray refinement, the coordination polyhedra of each atom have been determined and are shown in Figure 4. Uranium atoms are located in a distorted "Si_4C_4"

DOI: 10.1021/acs.inorgchem.7b02901
Inorg. Chem. XXXX, XXX, XXX−XXX

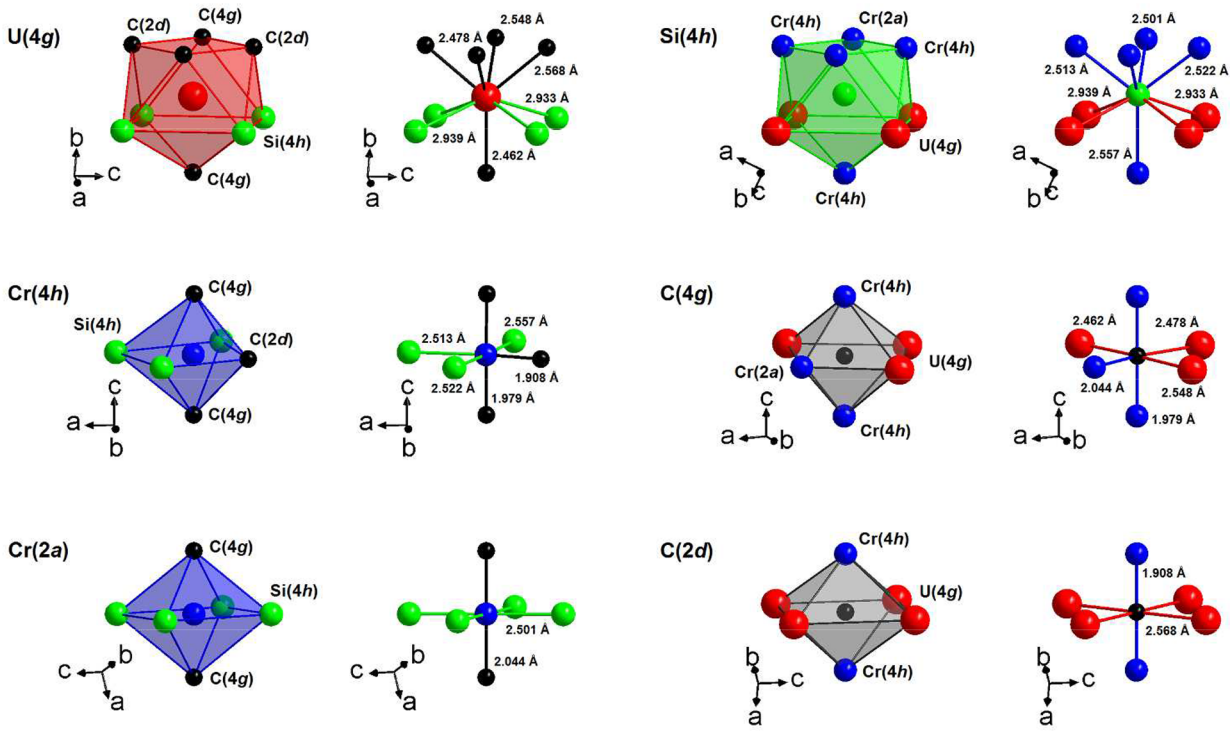

Figure 4. Coordination polyhedra in $U_2Cr_3Si_2C_3$.

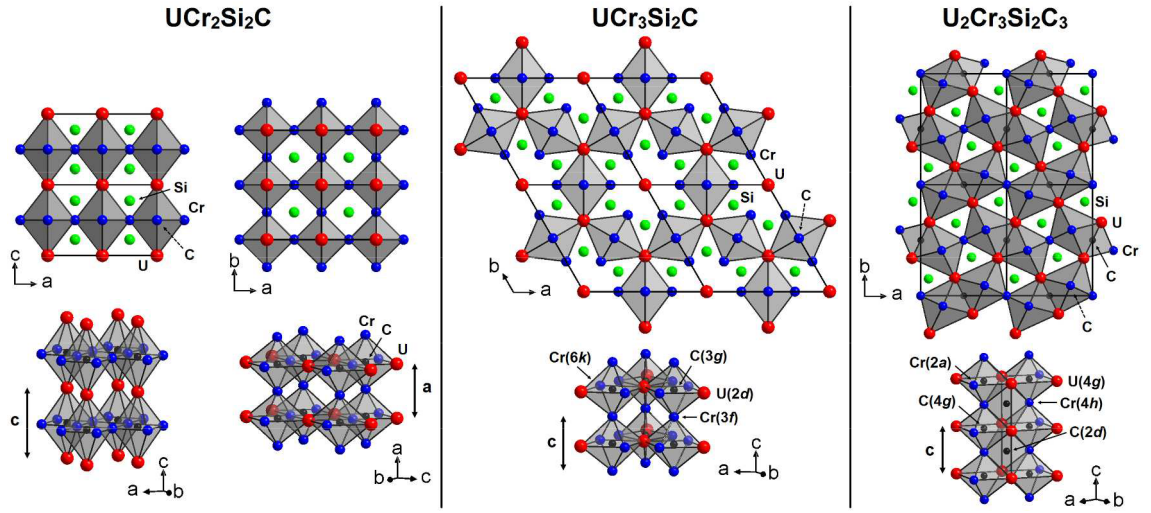

Figure 5. Comparison of the carbon-filled distorted-octahedral frameworks in UCr_2Si_2C, UCr_3Si_2C, and $U_2Cr_3Si_2C_3$.

antiprism face-capped by one carbon atom and silicon atoms in a distorted "U_4Cr_4"" antiprism face-capped by one chromium atom. Chromium atoms are located in strongly distorted "Si_3C_3" and "Si_4C_2" octahedra. Therefore, carbon atoms are located in strongly distorted "U_3Cr_3" and "U_4Cr_2" octahedra.

The refined cell parameters and atomic positions of $U_2Cr_3Si_2C_3$ are closely related to those encountered in the $Sc_2Pt_3Si_2$ compound (*Pbam*).[52] A full analysis of the structure clearly shows that $U_2Cr_3Si_2C_3$ must be considered as a carbon-filled variant of $Sc_2Pt_3Si_2$. However, it is worth noting that attempts to prepare $U_2Cr_3Si_2$ failed and led to a mixture of U_2Cr_3Si, UCr_2Si_2, and Cr_3Si phases, indicating the primordial role of carbon atoms in the structural stability of $U_2Cr_3Si_2C_3$.

Structural Relationships among UCr_2Si_2C, UCr_3Si_2C, and $U_2Cr_3Si_2C_3$. An octahedral environment is usually encountered around carbon atoms in ternary or quaternary uranium carbides: for example, "CU_6" octahedra in $U_{20}Si_{16}C_3$,[51] $U_6Co_{12}Ge_4C$.[53] or $U_6Fe_{16}Si_7C$,[54] "CU_5Si" in $U_3Si_2C_2$,[51] "CU_4Mn_2" in UMn_2SiC,[55] and "$CU_2(Fe,Si)_4$" in $U_2(Fe,Si)_{17}C_x$.[56] Carbon-centered "CU_4Cr_2" and "CU_3Cr_3" octahedra are also found in $UCrC_2$.[57] Similarly, one common feature in the three UCr_2Si_2C, UCr_3Si_2C, and $U_2Cr_3Si_2C_3$ quaternary compounds is the fact that carbon atoms are always located in distorted octahedra of uranium and chromium atoms (Figure 5). Hence, the crystal structure of UCr_2Si_2C can be described by the stacking along the *c* axis of carbon-centered distorted-octahedral "CU_2Cr_4" layers (left part of Figure 5). These octahedra share chromium atoms in the *a* axis and *b* axis directions to form square-framework octahedral layers and uranium atoms in the *c* axis direction. The silicon atoms

DOI: 10.1021/acs.inorgchem.7b02901
Inorg. Chem. XXXX, XXX, XXX−XXX

complete the structure by filling the distorted "U_4Cr_4" antiprism generated by the square framework of distorted carbon-centered octahedra "CU_2Cr_4".

The crystal structure of UCr_3Si_2C can also be described by the stacking along the *c* axis of carbon-centered distorted-octahedral "CU_2Cr_4" layers (middle part of Figure 5). In this crystal structure, the octahedra share in the (*a*,*b*) plane one U atom with two other carbon-centered distorted octahedra "CU_2Cr_4" to form hexagonal-framework octahedral layers. These hexagonal layers stack along the *c* axis by sharing Cr(3f) atoms. The remaining Cr(6k) atoms are involved with the Si atoms in the coordination polyhedra of the U(1a) and U(2e) atoms. The silicon atoms complete the structure by filling the distorted "U_2Cr_4" prismatic polyhedra (face-capped by Cr(3f) and U(1a)/U(2e) atoms) formed by the hexagonal framework of carbon-centered distorted octahedra "CU_2Cr_4".

The crystal structure of $U_2Cr_3Si_2C_3$ can be described by the stacking of infinite chains (main axis along the [001] direction) formed by two different carbon-centered distorted polyhedra (right part of Figure 5). Each chain is formed by (i) the association of two carbon-centered distorted octahedra "CU_3Cr_3" sharing one edge through two U(4*g*) atoms in the (*a*,*b*) plane and (ii) the stacking along the *c* axis of these bioctahedra by sharing chromium Cr(4h) atoms. Such stacking generates distorted "U_4Cr_2" octahedra which are filled by the C(2d) atoms. These second octahedra are then stacked along the *c* axis by sharing one edge through two U(4g) atoms and share "U_2Cr" faces with the carbon-centered distorted octahedra "CU_3Cr_3". These chains share the Cr(2a) atoms along the *a* axis and the U(4g) atoms along the *b* axis to form a complex three-dimensional framework of carbon-centered distorted octahedra "CU_3Cr_3" and "CU_4Cr_2". Finally, the crystal structure is completed by the Si atoms located in the distorted antiprisms formed by the complex carbon-filled distorted-octahedral framework.

The main interatomic distances, calculated from single-crystal X-ray diffraction at room temperature, and their relative evolutions in UCr_2Si_2C, UCr_3Si_2C, and $U_2Cr_3Si_2C_3$ are gathered for comparison in Table 3. As already mentioned, the structural stability of the quaternary U-Cr-Si-C compounds is mainly based on strong Cr−C and Cr−Si chemical bonds and weak U−C and U−Si chemical bonds. These results support the crystal structure descriptions based on the coordination octahedra of carbon atoms (Figure 5).

However, some differences among the three compounds could be noted. First, $U_2Cr_3Si_2C_3$ evidences the shortest Cr−C and U−C interatomic distances, while the Cr−Si interatomic distances are slightly longer in comparison to those calculated in UCr_2Si_2C and UCr_3Si_2C. This suggests that carbon atoms play an important role in the structural stability of $U_2Cr_3Si_2C_3$ and explains the nonexistence of the ternary $U_2Cr_3Si_2$ compound. Second, UCr_2Si_2C is the only U-Cr-Si-C quaternary compound with Si−Si interatomic distances shorter than the sum of the metallic radii, indicating chemical bonds between these atoms in this compound. Third, UCr_3Si_2C evidences very short Cr−Cr interatomic distances in comparison to UCr_2Si_2C and $U_2Cr_3Si_2C_3$, suggesting chemical bonds between chromium atoms in the former compound while this is not expected in the two other compounds. Fourth, $U_2Cr_3Si_2C_3$ and UCr_3Si_2C present slightly shorter U−Si interatomic distances in comparison to those encountered in UCr_2Si_2C. Finally, among the three quaternaries reported here in the U-Cr-Si-C system, $U_2Cr_3Si_2C_3$ evidences the shortest U−U interatomic distances, especially that of 3.275(1) Å, which is close to the sum of the metallic radius (Δ = +5.0%) and below the Hill limit (U−U spacing ≤ 3.5 Å),[58] suggesting the overlap of 5f wave functions and consequently the absence of magnetic ordering on the uranium substructure.

Table 3. Main Interatomic Distances at Room Temperature and Their Relative Evolutions in UCr_2Si_2C, UCr_3Si_2C, and $U_2Cr_3Si_2C_3$

	UCr_2Si_2C		UCr_3Si_2C		$U_2Cr_3Si_2C_3$	
	d_{ij} (Å)	Δ_{ij} (%)[a]	d_{ij} (Å)	Δ_{ij} (%)[a]	d_{ij} (Å)	Δ_{ij} (%)[a]
Cr−C	1.991	−12.5	1.951	−14.3	1.908	−16.2
			2.002	−12.0	1.979	−13.0
					2.044	−10.2
Cr−Si	2.446	−8.7	2.440	−8.9	2.501	−6.6
			2.478	−7.5	2.513	−6.2
					2.522	−5.9
					2.557	−4.6
U−C	2.580	+4.2	2.589	+4.6	2.462	−0.6
					2.478	+0.1
					2.548	+2.9
					2.568	+3.7
U−Si	3.045	+5.8	2.921	+1.5	2.933	+1.9
			3.016	+4.8	2.939	+2.1
Si−Si	2.319	−12.1	2.921	+10.7	3.061	+16.0
Cr−Cr	2.816	+3.5	2.533	−6.9	2.812	+3.4
			2.795	+2.8		
U−U	3.983	+27.7	4.003	+28.3	3.275	+5.0
					3.879	+24.3

[a] $\Delta_{ij} = 100[d_{ij} - (r_i + r_j)]/(r_i + r_j)$.

Crystal Structure of the Low-Temperature Form of UCr_2Si_2. As already mentioned in the Introduction, the low-temperature crystal structure of UCr_2Si_2 reported by Matsuda et al. appears ambiguous.[30] We have thus decided to reanalyze the structural transition and the low-temperature crystal structure of UCr_2Si_2 by using both powder and single-crystal X-ray diffraction.

PXRD patterns of UCr_2Si_2 have been recorded at room temperature (RT) and 150 K (Figure S2 in the Supporting Information). The RT pattern presents diffraction peaks characteristic of the $ThCr_2Si_2$ structure type, and its Rietveld refinement leads to cell parameters *a* = 3.910(1) Å and *c* = 10.502(1) Å, which are in excellent agreement with those refined from single-crystal X-ray diffraction data (Table S1 in the Supporting Information). The PXRD pattern recorded at 150 K (Figure S2 in the Supporting Information) evidence a splitting of the diffraction peaks, confirming the structural transition at low temperature.[30]

A careful analysis of the PXRD data recorded at 150 K suggests that this pattern can be refined by using a monoclinic unit cell of *C*2/*m* space group with refined cell parameters *a* = 5.553(1) Å, *b* = 5.484(1) Å, *c* = 5.852(1) Å, and *β* = 116.28(1)°. In order to confirm the monoclinic description of the low-temperature form of UCr_2Si_2 in the *C*2/*m* space group, single-crystal X-ray diffraction measurement has been performed at 100 K. The data collection and structure refinement conditions are gathered in Table S1 in the Supporting Information. The data confirm that UCr_2Si_2-LT crystallizes in the monoclinic *C*2/*m* space group, with uranium, chromium, and silicon atoms on the 2a (0,0,0), 4h (0,*y*,1/2) and 4i (*x*,0,*z*) sites, respectively (Table 4 and Figure 6).

DOI: 10.1021/acs.inorgchem.7b02901
Inorg. Chem. XXXX, XXX, XXX−XXX

Table 4. Atomic Coordinates, Site Occupancies, and Isotropic and Anisotropic Displacement Parameters of UCr_2Si_2 Refined by Single-Crystal X-ray Diffraction at T = 100 K[a]

atom	site	x	y	z	occ	U_{11}	U_{22}	U_{33}	U_{13}	U(eq)
UCr_2Si_2 (R1 = 3.31%)										
U	2a	0	0	0	1.00	0.009(1)	0.010(1)	0.004(1)	0.003(1)	0.007(1)
Cr	4h	0	0.2504(10)	1/2	1.00	0.026(2)	0.021(2)	0.005(2)	0.004(2)	0.018(1)
Si	4i	0.3852(15)	0	0.7719(13)	1.00	0.021(3)	0.011(3)	0.011(3)	0.010(2)	0.013(2)

[a] $U_{12} = U_{23} = 0$.

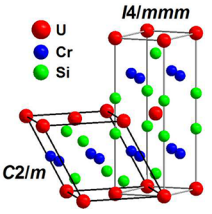

Figure 6. Representations of the high-temperature tetragonal ($I4/mmm$) and low-temperature monoclinic ($C2/m$) unit cells of UCr_2Si_2.

The structural transformation of UCr_2Si_2 occurring at low temperature is a simple lattice distortive displacement induced by a very weak movement of atoms (Figure 6). This displacive transformation from the high-temperature tetragonal form to the low temperature monoclinic form is supported by, on the one hand, the integrity of the single crystal used in XRD measurements at RT and 100 K and, on the other hand, by the number and the very close values of interatomic distances calculated from crystal structure refinements at 100 K and RT (Table S5 in the Supporting Information). Thus, as for UCr_2Si_2-RT, the crystal structure stability of UCr_2Si_2-LT is also mainly linked to the existence of strong Cr−Si and Si−Si chemical bonds.

Macroscopic Magnetic Measurements. The thermal variation of the magnetization of UCr_2Si_2, shown at the top of Figure S3 in the Supporting Information), confirms the antiferromagnetic ordering below T_N = 30(2) K.[22,30] This antiferromagnetic behavior is supported by the metamagnetic-like transition observed on the field dependence of the magnetization curves around μ_0H = 4, 6 T for T = 25, 20 K, respectively (bottom part of Figure S3 in the Supporting Information). At these temperatures, the maximum value of the magnetization (μ_0H = 9 T) reaches 0.4 μ_B, while at 5 K, the absence of a metamagnetic transition up to μ_0H = 9 T leads to a weak value of 0.09 μ_B (bottom part of Figure S3 in the Supporting Information). These results are in fair agreement with those measured on single crystals.[30]

UCr_2Si_2C, UCr_3Si_2C, and $U_2Cr_3Si_2C_3$ exhibit a Pauli paramagnetic behavior between 5 and 300 K (data not shown), suggesting no magnetic order of both chromium and uranium substructures in these quaternary uranium carbides. In order to reveal an eventual magnetic ordering, heat capacity measurements have been performed.

Heat Capacity Measurements. The specific heats of UCr_2Si_2C, UCr_3Si_2C, and $U_2Cr_3Si_2C_3$ have been measured from room temperature down to 2 K (Figure 7). The overall shape of the curves is compatible with the Debye model, and the absence of significant accident evidences the absence of magnetic ordering in this temperature range.

At 300 K, the specific heat of $U_2Cr_3Si_2C_3$ is not yet saturated and slowly converges to the Dulong and Petit limit (=3nR, where n is the number of atoms in the formula unit and R the ideal gas constant). This limit is only slightly exceeded for UCr_2Si_2C, which is not unusual for uranium-based intermetallics, this DP limit not taking into account the contribution of conduction and 5f electrons. The excess C_p for UCr_3Si_2C is more important, and extra contributions such as anharmonic vibrations must play a role in this compound.

With the absence of nonmagnetic thorium-based counterparts, it is difficult to extract precise values from these measurements. Nevertheless, one can estimate the Sommerfeld coefficients from the linear extrapolation to 0 K of $C_p/T = f(T^2)$ (inset to Figure 7a) at low temperature, yielding γ = 56, 53, 76 mJ mol_U^{-1} K^{-2} for UCr_2Si_2C, $U_2Cr_3Si_2C_3$, and UCr_3Si_2C, respectively. These electronic contributions are only moderately enhanced in comparison to regular metals and do not classify these compounds into the heavy Fermion family. The last value might also be slightly increased by the upturn

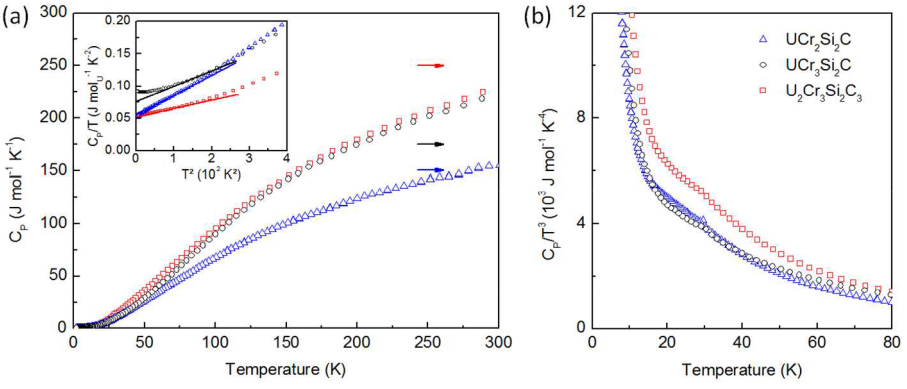

Figure 7. Thermal variation of the specific heats of UCr_2Si_2C (blue triangles), UCr_3Si_2C (black circles), and $U_2Cr_3Si_2C_3$ (red squares) plotted as (a) $C_p = f(T)$ and (b) $C_p/T^3 = f(T)$. The horizontal arrows mark the expected Dulong and Petit values at high temperature. The inset in (a) plots $C_p/T = f(T^2)$ per mole of uranium, and the solid lines highlight the linear behavior at low temperature.

DOI: 10.1021/acs.inorgchem.7b02901
Inorg. Chem. XXXX, XXX, XXX−XXX

observed below 100 K[2] and is often attributed to the influence of spin fluctuations in uranium-based intermetallics.

Finally, the $C_p/T^3 = f(T)$ curves for all three carbides exhibit a shoulder between 20 and 30 K. Such features are often attributed to soft optical Einstein modes with $\Theta_E \approx 5T_{max}$: i.e. $\Theta_E \approx 100-150$ K for the present carbides.[59]

Both macroscopic magnetic and heat capacity measurements suggest the absence of magnetic ordering in these quaternary carbides. However, as already mentioned in the Introduction, YCr_2Si_2, $LuCr_2Si_2$, and $ThCr_2Si_2$ were also reported to be Pauli paramagnets from only macroscopic measurements,[20−22] while neutron diffraction experiments reveal an antiferromagnetic order at very high temperature on the Cr substructure.[24−26] Hence, neutron diffraction appears to be the most powerful technique to determine the existence of magnetic order in these kinds of materials.

Powder Neutron Diffraction at Low Temperature. *UCr_2Si_2.* The refinements of the PND patterns of UCr_2Si_2 recorded at 280, 220, 60, and 2 K with $\lambda = 2.52$ Å are shown in Figure 8. The PND pattern recorded at $T = 280$ K only evidences the nuclear peaks of the tetragonal HT form ($ThCr_2Si_2$ structure type), while that recorded at $T = 60$ K only shows the nuclear peaks of the monoclinic LT form (own type of structure) (Figure 8). The diffraction pattern recorded at $T = 220$ K is characterized by a mixture of the HT and LT forms of UCr_2Si_2.

In order to precisely determine the temperature of the structural transition encountered in UCr_2Si_2, PND patterns have been recorded between 239 and 175 K (Figure S4 in the Supporting Information). These measurements show that the crystal structure transition from the tetragonal HT form to the monoclinic LT form starts between $T = 227$ K and $T = 220$ K and is complete at $T = 194$ K, in agreement with previous results.[30] These PND patterns can be perfectly refined considering only the nuclear Bragg peaks (Figure 8), indicating the absence of magnetic order on the chromium atoms at HT. The refined parameters of UCr_2Si_2 deduced from PND measurements are gathered in Table 5.

The refined atomic coordinates of both the HT and LT forms of UCr_2Si_2 are in agreement with those refined from single-crystal XRD data (Tables 1 and 4). The only exception concerns the refined parameters of the monoclinic form extracted from the 220 K neutron powder diffraction data (Table 5), but these values must be considered carefully due to the fact that at this temperature the monoclinic form is present in weak proportion in the sample (∼20%) beside the tetragonal form.

At $T = 2$ K, the appearance of purely magnetic diffraction peaks on the neutron pattern confirms the antiferromagnetic order of the uranium substructure (Figure 8). These magnetic peaks can be perfectly indexed with the magnetic space group $C\bar{1}$ and the propagation vector $k = [1,0,1/2]$. Considering the observed satellites $(hkl)^{\pm}$ with $h + k = 2n + 1$, the refinements have been performed by considering an anti-C Bravais lattice, leading to an antiferromagnetic arrangement of the uranium magnetic moments in the (001) plane. The best refinement is obtained with magnetic moments of uranium aligned perpendicularly to the (a,b) plane with a μ_U value of 0.66(5) μ_B at $T = 2$ K (Table 5). The magnetic structure of UCr_2Si_2 is shown in Figure 9.

UCr_3Si_2C. The PND pattern recorded at $T = 300$ K evidences the nuclear Bragg peaks of the hexagonal YCr_3Si_2C-type UCr_3Si_2C and diffraction peaks of weak intensity corresponding

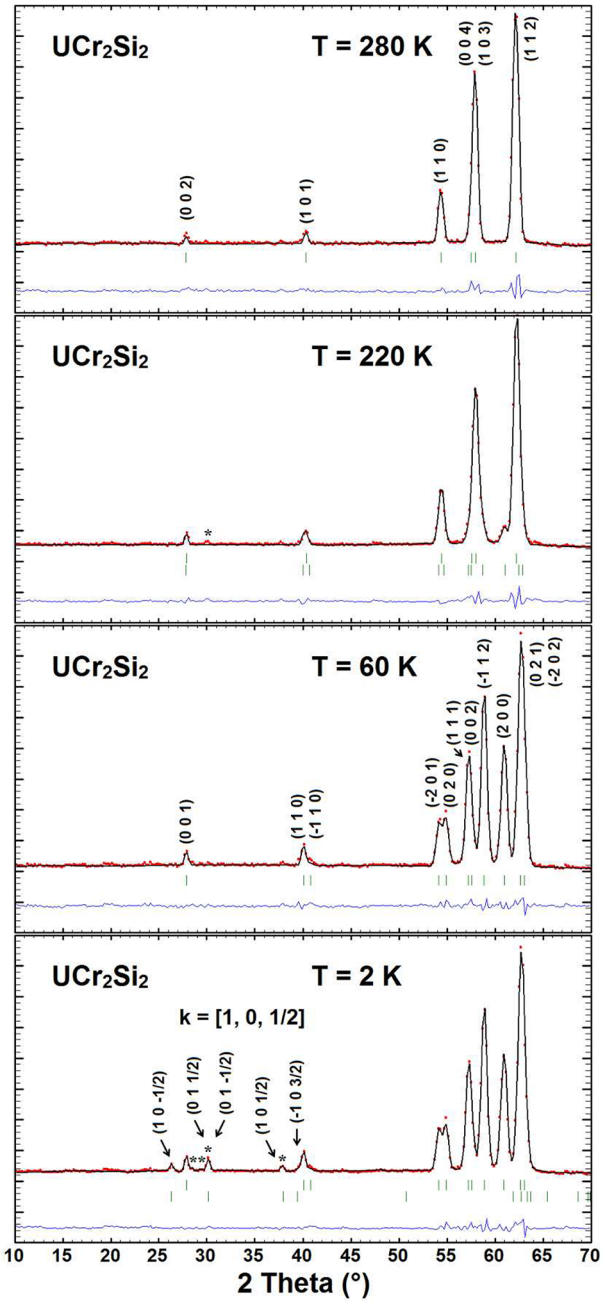

Figure 8. Refined powder neutron diffraction patterns of UCr_2Si_2 recorded at 280, 220, 60, and 2 K ($\lambda = 2.52$ Å). The asterisk refers to a $\lambda/2$ wavelength contribution.

to $U_2Cr_3Si_2C_3$ (Figure 10). The neutron pattern recorded at $T = 2$ K highlights neither magnetic contribution to the nuclear peaks nor extra magnetic diffraction peaks (Figure 10), indicating the absence of long-range magnetic order on both chromium and uranium substructures in UCr_3Si_2C (at least above 2 K) as suggested by magnetic and specific heat measurements.

The absence of magnetic ordering in this compound can be related to the crystallographic characteristics encountered in this type of structure. Indeed, the absence of magnetic ordering on the uranium substructure can be explained by the rather long U−U interatomic distances and the actinide substructure crystallographic disorder, while the absence of magnetic

DOI: 10.1021/acs.inorgchem.7b02901
Inorg. Chem. XXXX, XXX, XXX−XXX

Table 5. Refined Structural and Magnetic Parameters of UCr_2Si_2 from Powder Neutron Diffraction Measurements

		220 K			
	280 K			60 K	2 K
symmetry	tetragonal	tetragonal	monoclinic	monoclinic	monoclinic
space group	*I*4/*mmm*	*I*4/*mmm*	*C*2/*m*	*C*2/*m*	*C*2/*m*
a (Å)	3.901(2)	3.898(2)	5.542(3)	5.539(2)	5.540(1)
b (Å)			5.485(5)	5.468(2)	5.468(1)
c (Å)	10.477(6)	10.461(6)	5.846(5)	5.831(3)	5.830(2)
β (deg)			116.39(6)	116.24(2)	116.24(1)
V (Å^3)	159.4(2)	158.9(2)	159.2(3)	158.4(1)	158.4(1)
y_{Cr}	1/2	1/2	0.181(7)	0.217(2)	0.219(2)
x_{Si}	0	0	0.391(6)	0.400(2)	0.400(1)
z_{Si}	0.387(1)	0.386(1)	0.797(6)	0.775(1)	0.774(1)
μ_U (μ_B)					0.66(5)
R_{Bragg}; R_f	6.62; 4.71	5.00; 3.31	8.80; 5.19	4.50; 2.96	3.40; 8.39
R_{magn}					26.3
R_{wp}; R_{exp}; χ^2	2.65; 0.86; 9.44	2.17; 0.55; 15.3		1.83; 0.59; 9.77	1.61; 0.29; 30.2

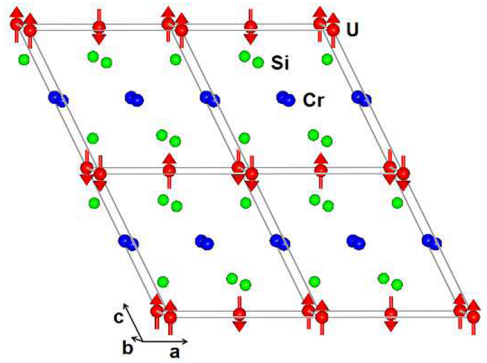

Figure 9. Representation of the magnetic structure of UCr_2Si_2 at T = 2 K.

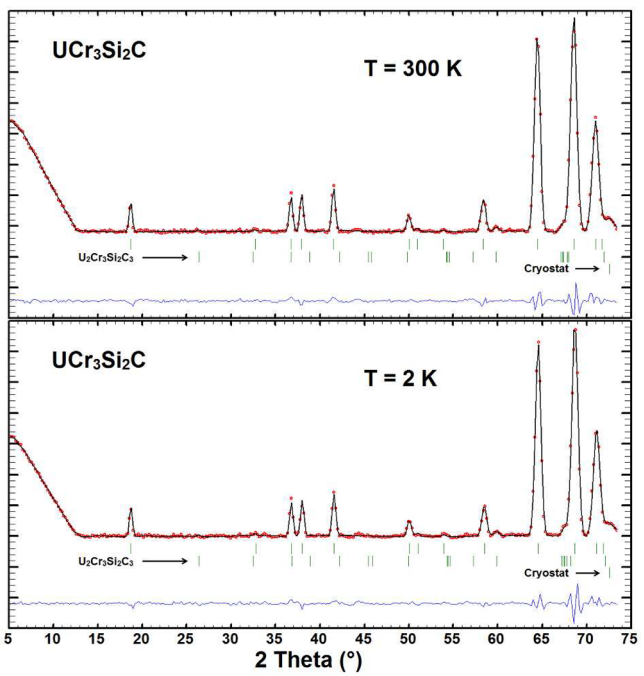

Figure 10. Refined powder neutron diffraction patterns of UCr_3Si_2C recorded at 300 and 2 K (λ = 2.52 Å).

ordering on the chromium substructure can be related to the very short Cr−Cr interatomic distances leading to strong chemical bonding between these atoms. As in the RCr_2Si_2C compounds, the absence of magnetic ordering on the chromium substructure can also be induced by the existence of strong hybridization between d states on Cr atoms and p states on carbon atoms.[33]

The PND patterns have been refined by fixing the atomic coordinates of $U_2Cr_3Si_2C_3$ and the z atomic coordinate of U(2e) in UCr_3Si_2C from those determined by single-crystal XRD data refinements (Table 2). The results of the refinements, gathered in Table 6, are in excellent agreement

Table 6. Refined Structural Parameters of UCr_3Si_2C from Powder Neutron Diffraction Measurements

	300 K	2 K
a (Å)	8.950(2)	8.934(2)
c (Å)	3.997(1)	3.994(1)
V (Å^3)	277.3(1)	276.1(1)
z_U(2e)	0.290	0.290
x_{Cr}(6k)	0.282(1)	0.281(1)
x_{Si}(6l)	0.187(1)	0.187(1)
f_{occ}(U(1a))	0.48(1)	0.48(1)
f_{occ}(U(2e))	0.24(1)	0.24(1)
R_{Bragg}; R_f	2.89; 2.36	2.33; 2.07
R_{wp}; R_{exp}; χ^2	2.22; 0.87; 6.49	2.34; 0.78; 9.10

with those obtained from single-crystal XRD data (Table 2). It is worth noting that, while the structural model used for single-crystal X-ray diffraction refinement leads to the substoichiometric chemical composition $U_{0.89}Cr_3Si_2C$ (Table 2), PND refinement leads to the almost stoichiometric chemical composition $U_{0.99}Cr_3Si_2C$ (Table 6).

UCr_2Si_2C. The PND patterns of UCr_2Si_2C recorded at T = 300 K and T = 2 K evidence the nuclear Bragg peaks of the tetragonal $CeCr_2Si_2C$ structure type and diffraction peaks of weak intensity corresponding to the UCr_3Si_2C and $U_2Cr_3Si_2C_3$ phases (Figure 11). The PND patterns were refined considering (i) the atomic coordinates of UCr_3Si_2C refined from PND data (Table 6) and (ii) the atomic coordinates of $U_2Cr_3Si_2C_3$ refined from single-crystal XRD data (Table 2). The refined structural parameters of UCr_2Si_2C (Table 7) are in

DOI: 10.1021/acs.inorgchem.7b02901
Inorg. Chem. XXXX, XXX, XXX−XXX

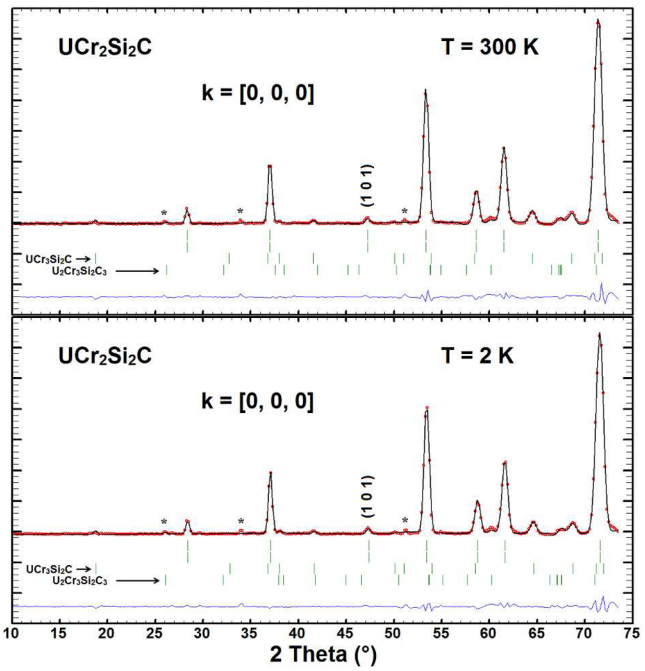

Figure 11. Refined powder neutron diffraction patterns of UCr_2Si_2C recorded at 300 and 2 K (λ = 2.52 Å). The asterisks refer to a $\lambda/2$ wavelength contribution.

fair agreement with those obtained from single-crystal XRD data (Table 1).

Table 7. Refined Structural and Magnetic Parameters of UCr_2Si_2C from Neutron Powder Diffraction Measurements

	300 K		2 K	
	$\|c$	$\|a$	$\|c$	$\|a$
a (Å)	3.968(1)	3.968(1)	3.964(1)	3.964(1)
c (Å)	5.146(1)	5.146(1)	5.134(1)	5.134(1)
V (Å^3)	81.0(1)	81.0(1)	80.7(1)	80.7(1)
z_{Si}	0.218(2)	0.218(2)	0.218(2)	0.218(2)
μ_{Cr} (μ_B)	0.56(5)	0.66(5)	0.58(5)	0.69(5)
R_{Bragg}	1.62	1.61	2.33	2.28
R_f	0.915	0.839	1.56	1.47
R_{magn}	14.1	3.17	19.8	7.91
R_{wp}	2.88	2.85	2.93	2.89
R_{exp}	0.62	0.62	0.38	0.38
χ^2	21.3	20.9	60.3	58.5

The PND patterns recorded at 300 and 2 K are similar (Figure 11), confirming the absence of magnetic transition between these temperatures as observed on $C_p(T)$ curves (Figure 7). Nevertheless, the crystal structure of UCr_2Si_2C leads to a nuclear contribution close to 0 for the (101) diffraction peak, while a non-negligible intensity is experimentally observed (Figure 11). This indicates a magnetic contribution to the (101) nuclear Bragg peak at both 300 and 2 K. In UCr_2Si_2C, the chromium atoms occupy the special position 2e (0,1/2,1/2), implying that Cr atoms are linked by a C Bravais mode. Hence, a magnetic contribution to the nuclear Bragg peaks (hkl) with $h + k = 2n + 1$ indicates an anti-C ordering, leading to an antiferromagnetic arrangement of the Cr magnetic moments within the (001) planes. This kind of magnetic arrangement, denoted AFl for antiferromagnetic layer, was observed in the $ThCr_2Si_2$-type RCr_2Si_2 (R = Tb, Ho, Er, Th) compounds.[24−26] However, in RCr_2Si_2 the AFls are antiferromagnetically coupled one with each other along the c axis,[24−26] while in UCr_2Si_2C they are ferromagnetically coupled (Figure 12).

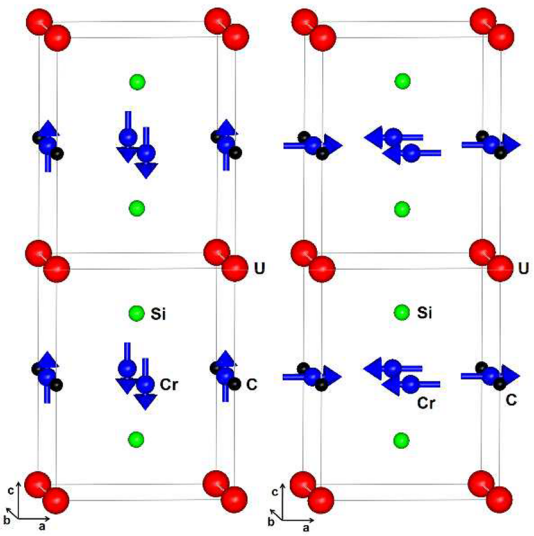

Figure 12. Representations of the possible magnetic structures of UCr_2Si_2C determined from neutron powder diffraction: (left) with an axial orientation of the Cr magnetic moments; (right) with a planar orientation of the Cr magnetic moments.

At this step, the magnetic structure can be refined considering either the Cr magnetic moments along the c axis (axial orientation) or perpendicular to the c axis (planar orientation). For a given temperature, the refinement for a planar orientation of the Cr magnetic moments yields a smaller R_{magn} value in comparison to that obtained for an axial orientation of the Cr magnetic moments (Table 7). Regardless of the temperature, the refined values of the Cr magnetic moments are very close for the same magnetic moments orientation (Table 7). This suggests that the Cr substructure in UCr_2Si_2C orders magnetically well above room temperature and that a planar orientation of the Cr magnetic moments is favored. However, an axial orientation is not excluded, and thus, the exact orientation of the magnetic moments cannot be determined unambiguously from powder neutron diffraction only. Therefore, alternative magnetic susceptibility measurements at high temperature and single-crystal neutron diffraction characterizations would be necessary to determine the Néel temperature and the exact orientation of the magnetic moments in UCr_2Si_2C. Nevertheless, these data highlight the antiferromagnetic ordering of the Cr substructure and the absence of magnetic ordering on that of U in UCr_2Si_2C, while the inverse is observed in the other compounds of the RCr_2Si_2C series involving a magnetic rare-earth element.[33,37] Such discrepancies between rare-earth- and uranium-based isostructural intermetallics are mostly due to the much larger extent of the 5f orbitals from the actinide in comparison to the 4f orbitals, inducing a much stronger hybridization with the neighboring atoms and greatly different band structures and magnetic interactions.

DOI: 10.1021/acs.inorgchem.7b02901
Inorg. Chem. XXXX, XXX, XXX−XXX

CONCLUSIONS

The crystallographic structures of the quaternary UCr_2Si_2C ($CeCr_2Si_2C$-type), UCr_3Si_2C (YCr_3Si_2C-type), and $U_2Cr_3Si_2C_3$ (its own type of structure) compounds have been determined by single-crystal X-ray diffraction and confirmed by powder X-ray and neutron diffraction studies. These three crystal structures are closely related to the ternary $CeMg_2Si_2$-, YCo_3Ga_2-, and $Sc_2Pt_3Si_2$-types, respectively, by the full occupancy of octahedral interstitial sites by carbon atoms. Our crystallographic results show that the structural stability of these three quaternary U-Cr-Si-C compounds is mainly based on strong Cr−C and Cr−Si chemical bonds and weak U−C and U−Si chemical bonds. One common feature in these three U-Cr-Si-C quaternaries is the localization of carbon atoms in distorted octahedra of uranium and chromium atoms: namely, "U_2Cr_4" in UCr_2Si_2C and UCr_3Si_2C and "U_3Cr_3" and "U_4Cr_2" in $U_2Cr_3Si_2C_3$. These results highlight the important role played by carbon atoms in their structural stability.

Magnetic and heat capacity measurements performed from room temperature down to 2 K do not show anomalies connected to any magnetic ordering in the carbides. Powder neutron diffraction experiments confirm these results except for UCr_2Si_2C, where an unexpected AFl magnetic order of the Cr substructure is revealed (i.e., antiferromagnetic arrangement of the Cr magnetic moments within the (001) planes) with a Néel temperature well above room temperature. Such a kind of magnetic arrangement has already been observed in RCr_2Si_2 (R = Tb, Ho, Er, Th) phases. However, in UCr_2Si_2C the AFls are ferromagnetically coupled along the *c* axis, while they are antiferromagnetically coupled in the RCr_2Si_2 compounds. Moreover, the antiferromagnetic ordering of the Cr substructure and the absence of magnetic ordering of that of U in UCr_2Si_2C (above 2 K) are unique among the RCr_2Si_2C series, where a ferromagnetic ordering of the lanthanide substructure at low temperature ($T_C \leq 30$ K) and the absence of magnetic order of that of chromium is usually observed.

Finally, single-crystal and powder X-ray diffraction reinvestigations of the low-temperature crystallographic form of UCr_2Si_2 ($T_t \approx 210$ K), previously reported in the triclinic $P\bar{1}$ space group, indicate that this compound crystallizes in the monoclinic $C2/m$ space group. Consequently, its magnetic structure has been reinvestigated from powder neutron diffraction data.

ASSOCIATED CONTENT

Supporting Information

The Supporting Information is available free of charge on the ACS Publications website at DOI: 10.1021/acs.inorgchem.7b02901.

Details on the data collection, structure refinement conditions, and main interatomic distances in UCr_2Si_2, UCr_2Si_2C, UCr_3Si_2C, and $U_2Cr_3Si_2C_3$, powder X-ray and neutron diffraction patterns of the tetragonal and monoclinic forms of UCr_2Si_2, and magnetic data of UCr_2Si_2 (PDF)

Accession Codes

CCDC 1585507−1585511 contain the supplementary crystallographic data for this paper. These data can be obtained free of charge via www.ccdc.cam.ac.uk/data_request/cif, or by emailing data_request@ccdc.cam.ac.uk, or by contacting The Cambridge Crystallographic Data Centre, 12 Union Road, Cambridge CB2 1EZ, UK; fax: +44 1223 336033.

AUTHOR INFORMATION

Corresponding Author

*E-mail for P.L.: Pierric.lemoine@univ-rennes1.fr.

ORCID

Pierric Lemoine: 0000-0002-3465-7815

Notes

The authors declare no competing financial interest.

ACKNOWLEDGMENTS

The authors gratefully thank T. Guizouarn for heat capacity measurements and Silvia Capelli for her valuable help in recording the neutron patterns. The authors are indebted to the Institut Laue Langevin (Grenoble, France) for the provision of research facilities (proposal 5-31-1949).

REFERENCES

(1) Ban, Z.; Sikirica, M. The crystal structure of ternary silicides ThM_2Si_2 (M = Cr, Mn, Fe, Co, Ni and Cu). *Acta Crystallogr.* **1965**, *18*, 594.

(2) Szytula, A.; Leciejewicz, J. Magnetic properties of ternary intermetallic compounds of the RT2 × 2 type. In *Handbook on the Physics and Chemistry of Rare Earths*; Gschneidner, K.A., Jr., Eyring, L., Eds.; North-Holland: Amsterdam, 1989; Vol. *12*, Chapter 83.

(3) Szytula, A. Magnetic properties of ternary intermetallic rare-earth compounds. *In Handbook of Magnetic Materials*; Buschow, K. H. J., Ed.; North-Holland: Amsterdam, 1991; Vol. *6*, Chapter 2.

(4) Gignoux, D.; Schmitt, D. Magnetism of compounds of rare-earths with non-magnetic metals. In *Handbook of Magnetic Materials*; Buschow, K. H. J., Ed.; North-Holland: Amsterdam, 1997; Vol. *10*, Chapter 2.

(5) McCall, W. M.; Narasimhan, K. S. V. L.; Butera, R. A. Magnetic properties of RCo_2Ge_2 compounds (R = La, Ce, Pr, Nd, Sm, Gd, Tb, Dy, Ho, Er, Tm, Yb, Lu, and Y). *J. Appl. Phys.* **1973**, *44*, 4724.

(6) Yakinthos, J. K.; Routsi, Ch.; Ikonomou, P. F. Magnetic properties of ternary TCo_2Si_2 compounds (T = Gd, Tb, Dy, Ho, Er, Y). *J. Less-Common Met.* **1980**, *72*, 205.

(7) Umarji, A. M.; Noakes, D. R.; Viccaro, P. J.; Shenoy, G. K.; Alfred, A. T.; Niarchos, D. Magnetic properties of $REFe_2Si_2$ compounds. *J. Magn. Magn. Mater.* **1983**, *36*, 61.

(8) Bud'ko, S. L.; Islam, Z.; Wiener, T. A.; Fisher, I. R.; Lacerda, A. H.; Canfield, P. C. Anisotropy and metamagnetism in the RNi_2Ge_2 (R = Y, La-Nd, Sm-Lu) series. *J. Magn. Magn. Mater.* **1999**, *205*, 53.

(9) Avila, M. A.; Bud'ko, S. L.; Canfield, P. C. Anisotropy magnetization, specific heat and resistivity of RFe_2Ge_2 single crystals. *J. Magn. Magn. Mater.* **2004**, *270*, 51.

(10) Narasimhan, K. S. V. L.; Rao, V. U. S.; Bergner, R. L.; Wallace, W. E. Magnetic properties of RMn_2Ge_2 compounds (R = La, Ce, Pr, Nd, Gd, Tb, Dy, Ho, Er, and Th). *J. Appl. Phys.* **1975**, *46*, 4957.

(11) Szytula, A.; Szott, I. Magnetic properties of ternary RMn_2Si_2 and RMn_2Ge_2 compounds. *Solid State Commun.* **1981**, *40*, 199.

(12) Venturini, G.; Welter, R.; Ressouche, E.; Malaman, B. Neutron diffraction studies of $LaMn_2Ge_2$ and $LaMn_2Si_2$ compounds: evidence of dominant antiferromagnetic components within the Mn planes. *J. Alloys Compd.* **1994**, *210*, 213.

(13) Nowik, I.; Levi, Y.; Felner, I.; Bauminger, E. R. New multiple magnetic phase transitions and structures in RMn_2X_2, X = Si or Ge, R = rare earth. *J. Magn. Magn. Mater.* **1995**, *147*, 373.

(14) Venturini, G. Magnetic study of the compounds RMn_2Ge_2 (R = La-Sm, Gd) and $R_xY_{1-x}Mn_2Ge_2$ (R = La, Lu; $0 < x < 1$) above room temperature. *J. Alloys Compd.* **1996**, *232*, 133.

(15) Siek, S.; Szytula, A.; Leciejewicz, J. Crystals and magnetic structure of RMn_2Si_2 (R = Pr, Nd, Y) and YMn_2Ge_2. *Solid State Commun.* **1981**, *39*, 863.

(16) Venturini, G.; Welter, R.; Ressouche, E.; Malaman, B. Neutron diffraction study of the ferromagnetic to antiferromagnetic transition in $La_{0.3}Y_{0.7}Mn_2Ge_2$: Phenomenological description of the magnetic

DOI: 10.1021/acs.inorgchem.7b02901
Inorg. Chem. XXXX, XXX, XXX−XXX

behavior of Mn in $ThCr_2Si_2$ silicides and germanides. *J. Alloys Compd.* **1995**, *223*, 101.
(17) Venturini, G.; Malaman, B.; Ressouche, E. Magnetic ordering in ternary RMn_2Ge_2 compounds (R = Tb, Ho, Er, Tm, Lu) from neutron diffraction study. *J. Alloys Compd.* **1996**, *240*, 139.
(18) Venturini, G.; Malaman, B.; Ressouche, E. The x-T magnetic phase diagram of the $La_{1-x}Y_xMn_2Ge_2$ system by neutron diffraction study. *J. Alloys Compd.* **1996**, *241*, 135.
(19) Hofmann, M.; Campbell, S. J.; Kennedy, S. J.; Zhao, X. L. A neutron diffraction study of $LaMn_2Si_2$ (10−473 K). *J. Magn. Magn. Mater.* **1997**, *176*, 279.
(20) Omejec, L.; Ban, Z. Magnetic susceptibilities of ThM_2X_2 compounds (M = Cr, Mn, Fe, Co, Ni and Cu; X = Si and Ge). *Z. Anorg. Allg. Chem.* **1971**, *380*, 111.
(21) Dommann, A.; Hulliger, F.; Baerlocher, Ch New $ThCr_2Si_2$-type representatives, $LnCr_2Si_2$ (Ln = Sm, Tb-Lu). *J. Less-Common Met.* **1988**, *138*, 113.
(22) Hiebl, K.; Rogl, P.; Horvath, C.; Remschnig, K.; Noël, H. Magnetism and structural chemistry of $U_{1-x}Y_xCu_{2\pm y}Si_{2\mp y}$, $U_{1-x}Y_xCr_2Si_2$, and $U(Cu_{1-x}Cr_x)_2Si_2$ alloys. *J. Appl. Phys.* **1990**, *67*, 943.
(23) Ijjaali, I.; Venturini, G.; Malaman, B. Evidence of a magnetic moment on the transition metal sublattice in $RFe_{2-x}Cr_xSi_2$ compounds (R = Y, La, Nd, Tb; $0.25 \leq x \leq 1.75$). *J. Alloys Compd.* **1998**, *279*, 102.
(24) Moze, O.; Hofmann, M.; Buschow, K. H. J. Chromium sublattice magnetic ordering in a compound of the $ThCr_2Si_2$ type structure: $HoCr_2Si_2$. *J. Alloys Compd.* **2000**, *308*, 60.
(25) Moze, O.; Hofmann, M.; Cadogan, J. M.; Buschow, K. H. J.; Ryan, D. H. Magnetic order in RCr_2Si_2 intermetallics. *Eur. Phys. J. B* **2003**, *36*, 511.
(26) Szytula, A.; Penc, B.; Hofmann, M.; Przewoznik, J. Antiferromagnetism of $ThCr_2Si_2$. *Solid State Commun.* **2012**, *152*, 1027.
(27) Janatova, M.; Vejpravova, J. P.; Divis, M. Magnetic properties of RCr_2Si_2 compounds (R = Tb, Er). *J. Magn. Magn. Mater.* **2010**, *322*, 1140.
(28) Li, L.; Hutchison, W. D.; Huo, D.; Namiki, T.; Qian, Z.; Nishimura, K. Low-field giant reversible magnetocaloric effect in intermetallic compound $ErCr_2Si_2$. *Scr. Mater.* **2012**, *67*, 237.
(29) Li, L.; Hu, G.; Umehara, I.; Huo, D.; Hutchison, W. D.; Namiki, T.; Nishimura, K. Magnetic properties and magnetocaloric effect of $GdCr_2Si_2$ compound under hydrostatic pressure. *J. Alloys Compd.* **2013**, *575*, 1.
(30) Matsuda, T. D.; Metoki, N.; Haga, Y.; Ikeda, S.; Okubo, T.; Sugiyama, K.; Nakamura, N.; Kindo, K.; Kaneko, K.; Nakamura, A.; Yamamoto, E.; Onuki, Y. Single crystal growth and structural and magnetic properties of the uranium ternary intermetallic compound UCr_2Si_2. *J. Phys. Soc. Jpn.* **2003**, *72*, 122.
(31) Tang, C.; Fan, S.; Zhu, M. Structure and magnetic properties of $CeCr_2Si_2C$. *J. Alloys Compd.* **2000**, *299*, 1.
(32) Pohlkamp, M. W.; Jeitschko, W. Preparation, properties, and crystal structure of quaternary silicide carbides RCr_2Si_2C (R = Y, La-Nd, Sm, Gd-Ho). *Z. Naturforsch., B: J. Chem. Sci.* **2001**, *56*, 1143.
(33) Klosek, V.; Vernière, A.; Malaman, B.; Tobola, J.; Kaprzyk, S. Quenching of the magnetic moment of Cr in RCr_2Si_2 compounds upon filling with carbon. *Phys. Rev. B: Condens. Matter Mater. Phys.* **2008**, *78*, 104419.
(34) Janatova, M.; Vejpravova, J.; Divis, M.; Sechovsky, V. Crystal structure and magnetism of RCr_2Si_2C compounds (R = La, Ce, Pr). *Phys. B* **2008**, *403*, 2338.
(35) Janatova, M.; Vejpravova, J. P.; Divis, M. Magnetic properties of $PrCr_2Si_2C$ single crystal. *J. Appl. Phys.* **2009**, *105*, 07E105.
(36) Janatova, M.; Vejpravova, J. P.; Sechovsky, V.; Divis, M. Magnetic properties of $NdCr_2Si_2C$ single crystal. *J. Phys.: Conf. Ser.* **2010**, *200*, 032024.
(37) Janatova, M.; Vejpravova, J. P.; Prokleska, J.; Sechovsky, V.; Divis, M.; Isnard, O. Magnetism and magnetic structure of $NdCr_2Si_2C$. *J. Phys.: Conf. Ser.* **2010**, *251*, 012018.
(38) Lemoine, P.; Tobola, J.; Vernière, A.; Malaman, B. Crystal and electronic structures of the new quaternary RCr_3Si_2C (R = Y, Gd-Tm, Lu, U) compounds. *J. Solid State Chem.* **2013**, *201*, 293.
(39) Rodriguez-Carvajal, J. Recent advances in magnetic structure determination by neutron powder diffraction. *Phys. B* **1993**, *192*, 55.
(40) Roisnel, T.; Rodriguez-Carvajal, J. WinPLOTR: A windows tool for powder diffraction pattern analysis. *Mater. Sci. Forum* **2001**, *378−381*, 118.
(41) Altomare, A.; Burla, M. C.; Camalli, M.; Cascarano, G.; Giacovazzo, C.; Guagliardi, A.; Moliterni, A. G. G.; Polidori, G.; Spagna, R. SIR97: a new tool for crystal structure determination and refinement. *J. Appl. Crystallogr.* **1999**, *32*, 115.
(42) Sheldrick, G. M. Crystal structure refinement with SHELXL. *Acta Crystallogr., Sect. C: Struct. Chem.* **2015**, *71*, 3.
(43) Farrugia, L. J. WinGX and ORTEP for Windows: an update. *J. Appl. Crystallogr.* **2012**, *45*, 849.
(44) Roisnel, T. local program (www.cdifx.univ-rennes1.fr/cryscalc).
(45) Marazza, R.; Ferro, R.; Rambaldi, G.; Zanicchi, G. Some phases in ternary alloys of thorium and uranium with the Al_4Ba-$ThCu_2Si_2$-type structure. *J. Less-Common Met.* **1977**, *53*, 193.
(46) Teatum, E.; Gschneidner, K.; Waber, J. In *The Crystal Chemistry and Physics of Metal and Alloys*; Pearson, W. B., Ed.; Wiley: New York, 1972.
(47) Troć, R.; Pasturel, M.; Tougait, O.; Potel, M.; Noël, H. Crystal structure and physical properties of a new intermetallics compound URu_2Al_{10}. *Intermetallics* **2011**, *19*, 913.
(48) Niemann, S.; Jeitschko, W. Ternary aluminides AT_2Al_{20} (A = rare-earth elements and uranium, T = Ti, Nb, Ta, Mo, and W) with $CeCr_2Al_{20}$-type structure. *J. Solid State Chem.* **1995**, *114*, 337.
(49) Bertaut, F.; Blum, P. La structure des borures d'uranium. *C. R. Hebd. Seances Acad. Sci.* **1949**, *229*, 666.
(50) Remschnig, K.; Le Bihan, T.; Noël, H.; Rogl, P. Structural chemistry and magnetic behavior of binary uranium silicides. *J. Solid State Chem.* **1992**, *97*, 391.
(51) Pöttgen, R.; Kaczorowski, D.; Jeitschko, W. Crystal structure, magnetic susceptibility and electrical conductivity of the uranium silicide carbides $U_3Si_2C_2$ and $U_{20}Si_{16}C_3$. *J. Mater. Chem.* **1993**, *3*, 253.
(52) Gribanov, A.; Grytsiv, A.; Rogl, P.; Seropegin, Y.; Giester, G. X-ray structural study of intermetallic alloys RT_2Si and $RTSi_2$ (R = rare-earth, T = noble metal). *J. Solid State Chem.* **2010**, *183*, 1278.
(53) Soudé, A.; Tougait, O.; Pasturel, M.; Kaczorowski, D.; Noël, H.; Roisnel, T. Characterization of the novel intermetallics compounds U_2Co_3Ge, $U_6Co_{12}Ge_4$ and $U_6Co_{12}Ge_4C$. *J. Alloys Compd.* **2011**, *509*, 5447.
(54) Berthebaud, D.; Tougait, O.; Potel, M.; Lopes, E. B.; Gonçalves, A. P.; Noël, H. Crystal structure and electronic properties of the new compounds $U_6Fe_{16}Si_7$ and its interstitial carbide $U_6Fe_{16}Si_7C$. *J. Solid State Chem.* **2007**, *180*, 2926.
(55) Hüfken, T.; Witte, A. M.; Jeitschko, W. Quaternary silicide carbide AT_2SiC (A = rare earth elements and actinides, T = Mn, Re, Ru, Os) with $DyFe_2SiC$-type structure. *J. Solid State Chem.* **1999**, *142*, 279.
(56) Chevalier, B.; Rogl, P.; Etourneau, J. R. Magnetic properties of the $U_2Fe_{17-x}M_xC_y$ intermetallic compounds with M = Al, Si, and Ge. *J. Solid State Chem.* **1995**, *115*, 13.
(57) Clark, N. J.; Mountford, R.; McColm, I. J. The coexistence of C_1 and C_2 species in carbides. Catenation defects. *J. Inorg. Nucl. Chem.* **1972**, *34*, 2729.
(58) Hill, H. H. In *Plutonium and Other Actinides*; Miner, W. N., Ed.; AIME: New York, 1970; Vol. 2.
(59) Winiarski, M. J.; Griveau, J.-C.; Colineau, E.; Wochowski, K.; Wiśniewski, P.; Kaczorowski, D.; Caciuffo, R.; Klimczuk, T. Synthesis and properties of $A_xV_2Al_{20}$ (A = Th, U, Np, Pu) ternary actinide aluminides. *J. Alloys Compd.* **2017**, *696*, 1113.

DOI: 10.1021/acs.inorgchem.7b02901
Inorg. Chem. XXXX, XXX, XXX−XXX